Spectroscopic fingerprints for charge localization in the organic semiconductor $(DOEO)_4[HgBr_4]\cdot TCE$

O.V. Koplak[1], A. Chernenkaya[2, 3, a)], K. Medjanik[3, 4], A. Brambilla[1], A. Gloskovskii[5], A. Calloni[1], H.-J. Elmers[3], G. Schönhense[3], F. Ciccacci[1], R.B. Morgunov[3]

[1]*Dipartimento di Fisica, Politecnico di Milano, 20133, Milano, Italy*
[2]*Graduate School Materials Science in Mainz, Staudingerweg 9, 55128, Mainz, Germany*
[3]*Institut für Physik, Johannes Gutenberg-Universität, D-55099 Mainz, Germany*
[4]*Lund University, MAX-lab, 22100 Lund, Sweden*
[5] *Deutsches Elektronen-Synchrotron DESY, Notkestr. 85, D-22607 Hamburg, Germany*

Changes of the electronic structure accompanied by charge localization and a transition to an antiferromagnetic ground state were observed in the organic semiconductor $(DOEO)_4[HgBr_4]\cdot TCE$. Localization starts in the temperature region of about 150 K and the antiferromagnetic state occurs below 60 K. The magnetic moment of the crystal contains contributions of inclusions (droplets), and individual paramagnetic centers formed by localized holes and free charge carriers at 2 K. Two types of inclusions of 100-400 nm and 2-5 nm sizes were revealed by transmission electron microscopy. Studying the temperature- and angular dependence of electron spin resonance (ESR) spectra revealed fingerprints of antiferromagnetic contributions as well as paramagnetic resonance spectra of individual localized charge carriers. The results point on coexistence of antiferromagnetic long and short range order as evident from a second ESR line. Photoelectron spectroscopy in the VUV, soft and hard X-ray range shows temperature-dependent effects upon crossing the critical temperatures around 60 K and 150 K. The substantially different probing depths of soft and hard X-ray photoelectron spectroscopy yield information on the surface termination. The combined investigation using complementary methods at the same sample reveals the close relation of changes in the transport properties and in the energy distribution of electronic states.

a) Author to whom correspondence should be addressed. Electronic mail: chernenk@uni-mainz.de.

I. INTRODUCTION:

Organic conductors are promising candidates for future molecular-scale memory applications. Reviews about the important practical applications and novelty of such materials were presented in [1-3]. The possibilities of molecular design through chemical synthesis and of miniaturizing dimensions are attractive properties of the molecular based conductors. Individual or small packets of molecules mounted within addressable cells conduct and switch electrical currents, and provide electrical bits of information [3]. Advantages of organic and polymer memories also include simplicity in device structure, good scalability, low fabrication costs, low-power operation, multiple properties interplay, and large capacity for data storage. Organic metals and semiconductors are strongly-correlated Fermi liquid systems manifesting unique physical properties such as charge and spin waves, unusual electrical and optical properties [4, 5]. Strong electron-electron correlations and electron – phonon interactions appearing due to low dimensional structure of the layered organic conductors cause unusual ground states of the crystals possessing a very rich spectrum of instabilities [4, 5]. Instabilities lead to metal-insulator or metal-semiconductor transitions controlled by the amount of Fermi surface involved in the electron-hole condensation.

Most of the organic conductors are layered two dimensional (2D) crystals whose symmetry contains an inversion center. The inversion symmetry forbids spin-orbit contribution like Aharonov-Bohm or Rashba-Bychkov effects. This paper is devoted to the quasi-2D organic conductor containing the asymmetrical DOEO molecule (1,4-(dioxandiil-2,3-dithio)ethylenedithiotetrathiafulvalene) packed in two dimensional layers. We have studied $(DOEO)_4[HgBr_4]\cdot TCE$ (where TCE is 1,1,2-trichloroethane) crystals (Fig. 1). The DOEO based crystals are layered systems attractive because conductive sheets of monomolecular thickness are separated by relatively large nonconductive zones of the anionic layer. Analogously to the family of BEDT-TTF cationic radical salts, the charge transfer from the DOEO layer amounts to 1 electron per molecular dimer. Synthesis, crystal structure, electrical and optical properties of the $(DOEO)_4[HgBr_4]\cdot TCE$ semiconductors were described in detail [6-9]. Raman scattering investigations showed that the crystalsare quasi-one dimensional (1D)conductors down to 140 K,whereas below this temperature the conductivity behavior becomes similar to the one typical forquasi-2D compounds [9]. Upon cooling the resistivity of the crystals increases until a maximum at ~ 140 K corresponding to a transition to the (anomalous) metallic state existing in the 70-140 K range. Below about 60 K a sharp increase of the resistivity was observed [6].The highest occupied molecular orbital (HOMO) of the DOEO molecule of π character constitutes a 2D valence band. An energy gap forms by two coupled DOEO molecules in the HOMO band. Therefore,the HOMO band is expected to be nominally quarter-filled.

The aims of this paper are: 1) identification of the particles contributing to magnetic and electrical properties in $(DOEO)_4[HgBr_4]\cdot TCE$ crystals; 2) studying the local symmetry of the crystal field in the region of the charge carrier localization; 3) identification of energy structure and chemical composition of the crystals by X-ray photoelectron spectroscopy (XPS) and hard X-ray photoelectron spectroscopy (HAXPES) in complicated multiphase system.

II. EXPERIMENTS

The $(DOEO)_4[HgBr_4]\cdot TCE$ crystals were of plate shape of ~1 mm^2 sizes. The structure of these crystals consists of alternating organic and inorganic layers (Fig. 1 b). The non-conducting inorganic layers are formed by $(HgBr_4)_2$ anions and TCE solvent molecules. The organic layers are built by dimerized DOEO molecular stacks (Fig. 1 a).

To investigate the high frequency spin dynamics and to separate contributions of particles of various types to the magnetic susceptibility of the crystal a Jeol JES FA200 electron spin resonance (ESR) spectrometer was used. The spectrometer operates in the X–band frequency range (9.013 GHz). The modulation frequency was 100 kHz, scanning range of the magnetic field was in the 0–16 kOe range. The temperature was varied in the 4 - 300 K range with a relative accuracy of ± 5% in an ESR 900 Oxford Instruments cryostat. The ESR spectra were recorded as dependences of the first derivative of microwave power absorption on the magnetic field, dP/dH. For measurements of the angular dependence the crystal was mounted on the sample holder with an absolute accuracy of $\pm 5^0$. Rotation of the sample in the cavity was carried out by a homemade goniometer with a relative error of $\pm 1^0$.

Ultraviolet and X-ray photoelectron spectroscopies (UPS and XPS, respectively) were used to determine the electronic and chemical properties of the compound. The XPS analysis utilized Mg $K\alpha$ radiation ($h\nu$=1253.6 eV), while hard X-rays were produced by the storage ring PETRA, Hamburg, thus providing two different scenarios of the probing depth. The combination of core- and valence photoemission spectroscopy is generally necessary for providing a full picture of the electronic structure. The XPS/UPS and HAXPES measurements were performed with two hemispherical analyzers (type SPECS Phoibos) for the standard and high-energy range, respectively. UPS employed a He discharge lamp (He I at 21.2 eV) for excitation. The full width at half maximum (FWHM) resolution was about 0.9 eV, 0.4 eV and 0.3 eV for XPS, HAXPES and UPS, respectively. All spectra were acquired at normal emission. The UHV sample manipulators were equipped with liquid helium cryostats, thus providing temperatures in the ca. 15-300 K range.

The HAXPES measurements were carried out at the P09 HAXPES end station of PETRA III (Hamburg) at a photon energy of 6000.5 eV [10, 11]. Due to the large inelastic mean free path of the fast electrons the probing depth was about 8 - 10 nm and thus surface contaminations or the termination of the surface play only a minor role. Comparison of XPS

and HAXPES spectra thus allows drawing conclusions about the surface termination of the as-grown crystals. Due to this large probing depth, more than one layer of DOEO molecules contributes to the photoelectron signal in the HAXPES measurements. So the interlayer conductivity might become visible in this spectral range. For maximum sensitivity and minimum radiation damage the energy analyzer (type SPECS Phoibos 225 HV) was combined with a delay-line detector (type Surface Concept). For the present measurements the overall energy resolution (electrons and photons) was 440 meV. The beam was focused down to 0.2 mm × 0.4 mm spot size. The spectra were recorded in normal emission geometry at nearly grazing photon incidence (≈ 2°).

Finally, the microstructure of the sample has been studied by transmission electron microscopy (TEM) using a Jeol JEM-2100 high resolution microscope.

III. RESULTS AND DISCUSSION

A. Magnetic properties

The ESR spectroscopy can indicate the localization of charge carriers via characteristic changes in the ESR spectrum, in particular spectral shape and symmetry. ESR gives information on the surroundings of the localized paramagnetic centers. For that reason ESR spectra of a $(DOEO)_4[HgBr_4]\cdot TCE$ crystal were recorded (Fig. 2). The ESR spectrum of $(DOEO)_4[HgBr_4]\cdot TCE$ crystal contains a line of Lorentz shape in the 4 – 300 K temperature range (Fig. 2 a). At higher temperatures, 70 – 300 K, this line possesses an axial angular dependence inherent to delocalized charge carriers in the organic conductors (Fig. 2 c).

Below T = 70 K the ESR spectrum is split into two anisotropic lines *1* and *2* (Fig. 2 b). The narrow line *1* (linewidth ~ 0.5 - 4 mT) which was also observed at high temperatures lies on the low-field wing of the wide line *2* (linewidth ~ 2 - 8 mT). Decomposition of the spectra recorded in different orientations into two Lorentz lines results in angular dependences of the *g*-factors of lines *1* and *2* (Fig. 2 c). Obvious differences of the angular dependences at 300 K and 5 K as well as pronounced differences between angular dependences of lines *1* and *2* indicate the presence of two distinct paramagnetic centers corresponding to different crystal fields. In Section D evidence will be presented that low temperature centers contribute to the ESR spectra by providing localized charge carriers.

A sharp increase of the sample resistivity below 70 K was observed in [6-9] and confirmed in special measurements for the crystal subjected to ESR studies. The room temperature dc conductivity of the crystal measured along the *a*-direction within the *ab* plane was R_{300} = 5 S/cm, while the perpendicular one was smaller by four orders of magnitude [6]. Upon cooling, the resistivity increases until a maximum is reached around 140 K. Below this maximum the

resistivity curve becomes metallic-type and finally undergoes an insulating transition at about 50 K. The resistivity of the sample R depends on the amount of delocalized charge carriers N_{del}: $1/R = N_{del}\mu ek$ (μ is mobility of the charge carriers, k is a geometric factor, e is the hole charge). Delocalized charge carriers (holes) do not strongly contribute to the magnetic moment of the sample M, because just a small part of them with energies close to the Fermi level E_F (softening zone ~ $4k_BT$) contributes to M. The number of localized holes $N_{loc} = (N - N_{del}) = N$- const/$R$ obeying the Curie law should predominantly contribute to M. The temperature dependence of N_{loc} (presented in arbitrary units) is shown in Fig. 3 a as well as the temperature dependence of magnetization M. The good correlation between N_{loc}(T) and M(T) dependences indicates the dominant contribution of the localized holes to the magnetic moment of the sample. The slight discrepancy between these curves may be explained by experimental details. A crystal was used for the measurement of the resistivity while the measurement of the temperature dependence of the magnetic moment by a SQUID magnetometer requires a large amount of sample material. To obtain the *M(T)* dependence about 8 mg of powder containing small crystals of ~ 0.1 mm sizes was used. Since the maximum of the $N_{loc}(T)$ curve varied from sample to sample, the magnetization corresponds to the average amplitude which is smaller than the one observed in individual samples. Provided a sufficient amount of material, magnetometry is a good tool for the estimation of the concentration of localized holes.

The main question implied to answer by magnetometry concerns the nature of the low temperature magnetic state of the localized carriers in the crystals. Measurements of the magnetic field dependence of the magnetization were performed to clarify this problem (Fig. 3 b). The Figure shows the field dependence of the $(DOEO)_4[HgBr_4]\cdot TCE$ molar magnetic moment. The experimental data was approximated using a sum of a linear function and a Brillouin function for the spin S [12]:

$$B_S(x) = \frac{2S+1}{2S}\coth\left(\frac{2S+1}{2S}x\right) - \frac{1}{2S}\coth\left(\frac{x}{2S}\right), \quad (1)$$

where

$$x = \frac{Sg_M\mu_B H}{k_B T}, \quad (2)$$

We assume that the Brillouin function is associated with a small amount of the impurities (i.e. unpaired and uncoupled spins) in the sample. The fit to the experimental data indicates a spin of S=10 corresponding to paramagnetic metallic nanoparticles. The linear term corresponds to the true susceptibility signal from the unpaired electrons within the crystal. The impurity component is very large at low fields and low temperatures compared to the linear component. Considering the absolute value of the total magnetic moment one obtains a different result. For the total magnetic

moment one must consider the saturated moment in infinitely large external magnetic fields. In this case the linear term becomes much larger (more than 95 %) than the impurity contribution. Subtracting the impurity contribution the magnetic susceptibility is almost constant, indicating the dominant temperature-independent Pauli paramagnetism due to delocalized electrons. The small deviation from the constant susceptibility above 50 K nicely fits to the temperature dependence of the number of localized electrons discussed above that provoke a Langevin-paramagnetism with spin S=1/2. A small maximum near 40 K might indicate the onset of antiferromagnetic order.

The crystal structure and low concentration of holes (one hole per molecular dimer [6-9]) explain the small value for the observed long range intermolecular exchange interaction because intermolecular distances exceed ~ 10 Å. The occurrence of antiferromagnetic long and short range order may explain the existence of a second ESR line *2* as an antiferromagnetic resonance. As an independent confirmation of this aspect one may see the different temperature dependence of the integral intensity of line *2* [13].

The occurrence of magnetic impurities requires additional confirmations which will be given in Section D.

B. X-ray photoelectron spectroscopy

XPS is very sensitive to the chemical composition and environment of the elements in a material in a probing depth typically about 1 nm. In XPS spectra, each element gives rise to a characteristic set of peaks in the photoelectron spectrum at kinetic energies determined by the photon energy and the respective binding energies. The presence of peaks at particular energies therefore indicates the presence of a specific element in the sample under study. Furthermore, the intensity of the peaks is related to the concentration of the element within the analyzed region. Thus, the technique provides a quantitative analysis of the surface composition. Arising out of the fact that the transfer of charge from the valence orbitals, typically involved in chemical bonding, is reflected in the measured binding energies of the core levels of the atoms, it is possible to distinguish the signals originating from atoms in different chemical environment.

The hard X-ray variant of XPS (HAXPES) provides the same information but for a substantially larger probing depth of 8-10 nm, corresponding to 5-7 DOEO layers of the title compound. HAXPES thus makes it possible to investigate the electronic structure in the bulk of the material. Furthermore, the comparison of bulk and surface photoelectron spectra gives information on the surface termination. A combined study using soft and hard X-ray photons on the same sample allows to discuss the electronic structure taking into account different structural aspects at the surface.

Along with the discussion of photoemission spectra we should mention two main phenomena that could contribute to the experimental HAXPES and XPS spectra besides the true signal of the organic material: radiation damage and charging of the crystals or parts of them. In order to avoid the effect of radiation damage, several crystals from different batches were measured in parallel at each temperature in our experiments. Furthermore, the X-ray beam was shifted to a new position at the sample before every new scan. Charging often occurs during measurements on insulating materials. The inhomogeneous charge distribution in the beam spot normally broadens the XPS signals and shifts the whole spectrum to lower kinetic energies. In XPS, we observe the charging effect very close (within about 1 nm) to the surface. However, in HAXPES the large mean free path of several DOEO layers can lead to inhomogeneous, layer-wise charging as discussed in [14]. The present results indeed show a charging contribution both in the XPS and HAXPES spectra that could not be avoided. The measurements were reproduced on several samples from different batches and spectra were taken both during cooling and during warming up from low temperatures. The trend for all samples was the same.

XPS and HAXPES spectra of $(DOEO)_4[HgBr_4]\cdot TCE$ crystals were taken in the temperature range 45 K – 300 K. The survey XPS spectrum of the DOEO salt taken at room temperature shows all the elements present in the material (Fig. 4 a). The spectrum contains the carbon, oxygen and sulfur signals corresponding to the conductive DOEO stack layers as well as mercury and bromine present in the anion sublattice and chlorine from the TCE solvent.

A HAXPES survey spectrum of the shallow core levels, recorded at room temperature, is shown in Fig. 5a. Like in the XPS case, the spectrum contains the signals of all DOEO components, however, with substantially different intensity ratios. This reflects the difference in the partial photoemission cross sections. We observe chlorine of the solvent molecules embedded in the anionic layer. At room temperature the signals are well resolved and non-split.

For further evaluation the Hg 4f and S 2p XPS lines are discussed as signatures of anion and cation, respectively (Fig. 4 b, c). In case of HAXPES the Hg 4d, S 2s and Cl 2p signals are used as a probe for the anion, the DOEO molecule and the solvent component, respectively (Fig. 5 b). All evaluated lines are well suitable for the quantitate discussion, because their intensities are large and the component structure is very pronounced. The decrease of HAXPES photoemission cross section with increasing kinetic energy is less pronounced for s-states than for higher angular momentum states. Hence it was possible to study the S 2s level at good intensity.

Let us now compare the relative intensities of the anionic components mercury and bromine. Their intensities in the HAXPES survey spectrum are much higher than those for the surface-sensitive XPS in comparison to signals of C 1s and O 1s that have the largest intensities in the spectra (see Figs. 4 a and 5 a). The S/Hg and S/Br XPS ratios calculated using the experimental data and cross section constants from Ref. 16 are higher than expected from the composition,

suggesting that the surface of the as-grown crystals is mainly terminated by the layer of DOEO molecules. HAXPES, with its large probing depth, gives spectroscopic access to the buried anionic layers. This general finding of termination of the surface by the DOEO layer is in agreement with results from scanning tunneling spectroscopy (STS) on the related compound $(BEDT\text{-}TTF)_2Cu[N(CN)_2]Br$, where tunneling spectra of as-grown crystals gave direct evidence of the states in the cationic layers in the superconducting phase [15].

Due to non-monotonic behavior of transport [6] and spin properties [13], it is interesting to follow the development of the photoemission spectra with cooling. At 200 K the Hg 4f XPS spectrum (Fig. 4 b) displays the Hg 4 f7/2 and 4 f5/2 spin-orbit doublet appearing at 100.5 and 104.5 eV, respectively. The additional third peak showing up in the Hg 4f region, located at 102.2 eV, can be associated with Si oxides, whose presence is likely due to surface contaminants. The HAXPES line shown in Fig. 5 b, presenting the same element of the anion, is Hg 4d. It shows also a fine-structure doublet of Hg $4d_{3/2}$ and Hg $4d_{5/2}$. In the HAXPES spectra of Hg we do not observe a further splitting at room temperature, because the surface contribution is very small in comparison to the bulk contribution of several anionic layers. Furthermore, we do not observe a signal from Si (at about 102 eV BE) in the bulk, proving the appearance of this line in XPS due to surface features. The HAXPES spectrum of Cl 2p, which is also a fingerprint of the anionic layer (where also the TCE solvent molecules are located), at 200 K consists of a single line. Normally, the Cl 2p has two contributions located at about 200 and 202 eV of binding energy due to the spin-orbit splitting. In the present experiment we could not resolve this difference. A main contribution to peak broadening is associated with the rich phonon spectra of the title compound, in addition to lifetime broadening effects.

The S 2p XPS level (see Fig. 4 c) at 200 K is the convolution of a spin-orbit split doublet in which the binding energies of the S $2p_{3/2}$ and the S $2p_{1/2}$ core levels are 164.2 eV and 165.3 eV, respectively, and of another doublet, characterized by a significantly lower intensity, with binding energies of 165.4 eV and 166.5 eV for the $2p_{3/2}$ and $2p_{1/2}$ components, respectively. The presence of two S doublets can be associated either with photoemission from nonequivalent S sites in the DOEO molecule, or to the presence of DOEO molecules with different charge states. Similar observations are reported in the literature for the photoemission from organic salts (see e.g. [16] and references therein).

The S 2s HAXPES line at 200 K (Fig. 5 b) exhibits a low-energy satellite signal, shifted by about 4eV. This satellite becomes stronger at 130 K, although the Hg 4d and Cl 2p lines do not show an indication of charging. We thus believe that the S 2s satellite (at about 232 eV BE in Fig. 5 b) indicates a true chemical shift. When cooling the crystals down to 130 K and therefore crossing the transition temperature to the metallic regime, a shift of 0.4 eV in both Hg 4f

and S 2p XPS lines is observed. Similarly, there is a shift of about 1.5 eV to lower kinetic energies in all HAXPES spectra. The first sign of electron density redistribution between S 2s component lines in the bulk becomes visible.

Upon further cooling down to 70 K Hg 4f and S 2p surface signals do not change. In contrast, additional split lines in Cl 2p, Hg 4d3/2 and Hg 4d5/2 from the bulk of the crystals appear and the spectra are shifted further by 2.2 eV in the same direction to lower kinetic energies. The low-energy satellite of the S 2s HAXPES signal becomes significant in comparison to the higher temperatures.

Hereby, the observed shift of the XPS surface lines with cooling to 130 K is associated with surface charging of the crystal. The additional low-energy component of S 2s HAXPES signal from the bulk is a true chemical shift. Upon further cooling to 70 K the system becomes insulating and layer-wise charging is observed in the bulk, similar to the finding for $(TMTTF)_2SbF_6$ discussed in Ref. 14. Therefore, using both XPS and HAXPES we can follow and discuss not only surface vs. bulk differences, but also observe the interlayer conductivity change in the layered organic compound.

The hypothesis about a transition from 1D electrical conductivity (at high temperatures) to 2D conductivity (below 140 K) proposed in [9] stimulated us to study the temperature dependence of the electrical anisotropy. In order to quantify the electrical anisotropy we introduce the ratio $R_\perp/R_\parallel$ of the "out-of-plane" $R_\perp$ and "in plane" $R_\parallel$ resistivity using experimental data from Ref. 6.

Two facts become obvious from the comparison of temperature dependences of $R_\perp/R_\parallel$ and the XPS shift, both plotted in Fig. 6. Cooling of the crystal continuously increases the ratio $R_\perp/R_\parallel$ of the electrical conductivity towards two-dimensional behaviour. This continuous "transition" of the electrical dimensionality is accompanied with the localization of holes that, in turn, leads to dielectric polarization of the sample. The additional evidence of localization (besides the resistance behaviour itself [6-9]) is a significant shift of the XPS signals towards lower kinetic energies, progressively down to 140 K. The temperature dependence of the electrical anisotropy parameter $R_\perp/R_\parallel$ (triangles in Fig. 6) thus correlates with the temperature dependence of the level shifts in the XPS spectra (circles). In the DOEO layer the conductivity originates from transfer of holes between dimers through short contacts between "tail-to head" molecules whose ends contain sulphur atoms. Further, also the intensity ratio of the HAXPES signals (i.e. the ratio of the area of the shifted line and the total area of shifted and non-shifted line, squares) also follows this trend. The net charge accumulated in the near-surface region in the steady-state equilibrium during irradiation with the hard X-rays is an indirect measure of the interlayer conductivity.

C. Ultraviolet photoelectron spectroscopy

UPS probes the single-particle spectral function and is therefore a useful tool to investigate highly correlated systems. According to the atomic subshell photoionization cross sections calculated in [17], the contributions of the C 2p and S 3p orbitals are very large for the He I photon energy, whereas those of Hg 5d is rather small because of the small cross sections and small atomic ratios [18]. The work function Φ of DOEO was estimated from the onset of the secondary electrons, to be 4.1±0.2 eV. The work function of a semiconductor, however, is not solely determined by the ionization energy but also by the position of the Fermi level at the surface, which may be shifted by the occupation of surface states in the gap. From the estimated value of Φ and assuming an ionization energy E_I = 4.8 eV for the neutral DOEO molecules [7], it is possible to give an estimate of the expected position for the HOMO level, at a binding energy of 0.7±0.2 eV.

Figure 7 shows a series of UPS spectra of the $(DOEO)_4[HgBr_4]\cdot TCE$ crystal taken between 250 and 40 K in the valence-band region. All spectra exhibit a slow increase in the 2 to 4 eV region, where S 3p states are expected to give the dominant contribution [18, 19]. Between 4 and 11.5 eV there is a steep rise towards a pronounced peak at 11.5 eV. This peak stays fixed in energy, ruling out charging. In this range we expect a contribution also from Hg 5d, C 2p and S 3s states [18, 19]. The inset of Fig. 7 is an enlargement of the part of the spectrum denoted by a dashed rectangle. This region shows a significant dependence on temperature, see inset. The changes in the spectra are strong between 250 and 140 K and significantly lower between 120 and 40 K, i.e. there is a discontinuity at about 130K.

Photoemission and electronic structure near the Fermi level (E_F) in similar TTF- and BEDT-TTF-based crystals was studied by R. Liu et al. [19], Downes et al. [20] and Kiss et al. [21]. Significant photoelectron-emission intensities are observed in the region close to E_F, in those salts showing a metallic behavior. It turned out that the intensity at the Fermi edge depends strongly on the preparation process (cleavage) and samples from the same batch can show different behaviors, depending on the individual surface termination [20]. The spectra of Fig. 7 display zero intensity at the Fermi edge and until 0.5 eV below E_F, where metallic bands are expected. This may point on semiconductor behavior, and the negligible intensity at E_F would be caused by the presence of a gap. However, in the light of the results presented in [20], we refrain from a clear distinction of metallic or semiconducting behavior on the basis of Fig. 6.

The vibrational structure of the $DOEO^0$ neutral molecule, the $DOEO^+$ cation, and the TCE solvent molecule were described using the DFT method (density functional theory) in [7]. For fully optimized $DOEO^0$ the skeleton is non-planar, whereas for $DOEO^+$ it is almost planar (except for the outer ethylene groups). Computation of the electronic structure of $DOEO^0$ and $DOEO^+$ was performed using quantum-chemical calculations at different levels of theory,

revealing HOMO energy values of 4.8 eV and 8.5 eV as referred to the vacuum level (corresponding therefore to 0.7 eV and 4.4 eV in our reference system, respectively) for the neutral and charged $DOEO^{+}$ molecule, respectively. The theoretical LUMO energy (referred to the vacuum level) is about 1.3 eV for $DOEO^{0}$ and 7.2 eV for $DOEO^{+}$ [7]. If the conduction band originates from the HOMO in the $(DOEO)_4[HgBr_4]\cdot TCE$ salt, we would expect to have delocalized conduction electrons parallel to the stacking axis. The direct overlapping of the planar part of the DOEO molecule with an interplanar distance of 3.57 Å enables intermolecular electron transfer through the π orbitals.

D. Transmission electron microscopy and "droplets" contribution to the electrical and magnetic properties

HRTEM images with small and large magnification of a $(DOEO)_4[HgBr_4]\cdot TCE$ crystal are shown in Fig. 9 a, b. In Fig. 9a one observes inhomogeneous features that appear as droplets of 100-400 nm diameter covering about 20-30 % of the observed area. The dark appearance of the droplets indicates a large absorption of electrons which might be explained by a high Z contrast, i.e. the droplets contain a high concentration of a heavy element, e.g. Hg. The more homogeneous sections between the droplets reveal parallel lines with a distance of 3 nm indicating the separation of the cation layers. These structures form a mosaic pattern indicating a large number of dislocations in the molecular structure. The magnified image shows blocks of atomic planes separated from each other by 2.66 Å (Fig. 9 b). This length scale corresponds to the distance of DOEO molecules. Heterogeneities were revealed at room temperature but of course it is likely that they persist at low temperatures. It is well known that the instability of the crystal lattice as well as the small activation energy of dislocations and diffusion can result in a phase separation. It is reasonable to suppose that the "droplet" inclusions are amorphous and therefore remain invisible for structural investigations using X-ray diffraction. One should expect Schottky barriers forming on the droplet interface providing a Coulomb repulsion of the charge carriers balanced with equilibrium concentration of the holes in the crystal bulk. This is a way to explain the impurity component discussed for the magnetization measurements.

IV. CONCLUSIONS

At low temperature an antiferromagnetic phase of localized holes coexists with paramagnetic individual localized holes in $(DOEO)_4[HgBr_4]\cdot TCE$. The symmetry of the "islands" of the antiferromagnetic phase was found to be different in comparison with the symmetry of the ESR spectra of free charge carriers.

In the temperature region of 120-160 K the XPS spectra reveal characteristic level shifts of the order of 400 meV and the HAXPES spectra exhibit strongly shifted signals due to the buildup of non-equilibrium charge distribution in the near surface region. The XPS shifts reflect the surface charge within the first 1 nm, i.e. within the first DOEO layer. In

contrast, the HAXPES shifts arise from a probing depth of about 8-10 nm, i.e. 5-7 DOEO layers. The intralayer conductivity is much higher than the interlayer conductivity. Hence, electrostatic decoupling of adjacent layers occurs as discussed in [14], leading to several separated signals. The temperature dependences of the continuous XPS level shift and the intensity ratio of the shifted signal versus the unshifted signals in HAXPES spectra are in accordance with the conductivity anisotropy parameter $R_{\perp}/R_{\parallel}$.

The comparison of XPS and HAXPES spectra gives information on the surface termination. XPS (probing depth about 1nm) sees the surface and topmost DOEO layer, whereas HAXPES gives spectroscopic access to several buried cationic and anionic layers. The comparison indicates that the surface of the as-grown crystals is mainly terminated by the layer of DOEO molecules. In UPS spectra significant changes as function of temperature are observed between room temperature and about 130 K. At this temperature the variation levels off and is much smaller between 120 K and 40 K. The intensity at E_F is zero, which points on semiconducting behaviour. However, due to the small probing depth of UPS we cannot exclude a possible influence of surface termination or a different chemical state of the topmost DOEO layer.

Continuous localization of holes results in non-monotonous variations of the resistivity and magnetization of the samples corresponding to a competition between free charge carriers, individual localized holes and condensed droplets containing large amounts of spins. The obtained data can be used to explain extraordinary electrical and magnetic properties of the $(DOEO)_4[HgBr_4]\cdot TCE$ crystals. Appearance of an antiferromagnetic phase below 60 K in a non-magnetic compound not containing metal atoms is an evidence of the strong electron-electron correlation in this two-dimensional system.

ACKNOWLEDGMENTS

O.V.K. thanks Cariplo Foundation, R.B.M. thanks Mainz University for hospitality during a research visit. Financial support by DFG (Transregio SFB TR49), BMBF (05K13UM4) and Graduate School of Excellence MAINZ is gratefully acknowledged. The authors are grateful to I. Khodos for assistance in HRTEM measurements and to W. Drube with team for support during the measurements at beamline P09 (PETRA III at DESY, Hamburg). A.C. research is funded by Fondazione Cariplo (2012-09-04 SECARS project). Funding for the HAXPES instrument at beamline P09 by the Federal Ministry of Education and Research (BMBF) under contracts 05KS7UM1 and 05K10UMA with Universität Mainz; 05KS7WW3, 05K10WW1 and 05K13WW1 with Universität Würzburg is gratefully acknowledged.

Author Contributions: All authors contributed equally to this work. O.V.K., A.C. and A.B. performed the experiments on ESR, SQUID, XPS, HAXPES, UPS and TEM, K.M. was involved into the HAXPES investigation, A.G.

supervised HAXPES experiment at DESY, A.C. supervised UPS and TEM experiments, F.C., H.J.E., G.S. and R.M. supervised the work on all stages. All authors discussed the results and implications and commented on the manuscript at all stages.

REFERENCES

[1]. G. Saito and Y. Yoshida, Top Curr. Chem., **312**, 67(2012).

[2]. W. J. M. Naber, S. Faez and W. G. van der Wiel, J. Phys. D: Appl. Phys., **40**, R205(2007).

[3]. J. Singleton and Ch. Mielke, Contemporary Physics, **43**, 63(2002).

[4]. N. Toyota, M. Lang, J. Müller, Low-dimensional Molecular Metals, Springer Series in Solid-State Sciences, **154**, 1(2007).

[5]. F. Kagawa, T. Sato, K. Miyagawa, K. Kanoda, Y. Tokura, K. Kobayashi, R. Kumai& Y. Murakami, Nature Physics, **9**, 419 (2013).

[6]. A.A. Bardin, A.I. Kotov, S.S. Khasanov, G.V. Shilov, L.I. Buravov, L. Ouahab, E.B. Yagubskii, Coordination Chemistry, **32**, 88, (2006);

[7]. A. Lapinski, A.I. Kotov, Molecular Physics, **106**, 33 (2008).

[8]. A. Lapinski and A.I. Kotov, Chem. Phys., **326**, 551 (2006).

[9]. A. Lapinski, A. Gasecka, A. Graja, S. Waplak, A. Ostrowski, A. Kotov, Optical Materials, **34**, 1651 (2012).

[10]. J. Strempfer, S. Francoual, D. Reuther, D. K. Shukla, A. Skaugen, H. Schulte-Schrepping, T. Kracht and H. Franz: Journal of Synchrotron Radiation **20**, 541-549, (2013).

[11]. A. Gloskovskii et al., Journal of Electron Spectroscopy and Related Phenomena **185**, 47 (2012).

[12]. J. R. Anderson, G. Kido, Y. Nishina, M. Górska, L. Kowalczyk, Z. Golacki, Phys. Rev. B 41, 1014 (1990)

[13]. A. Chernenkaya, O. Koplak, A. Kotov, R. Morgunov, E. Yagubskii, Physics of the Solid State **54,**2391 (2012).

[14]. K. Medjanik, M. de Souza, D. Kutnyakhov, A. Gloskovskii, J. Müller, M. Lang, J.- P. Pouget, P. Foury-Leylekian, A. Moradpour, H. J. Elmers and G. Schönhense, European Phys. J. B, **87**, 256 (2014).

[15]. S. Diehl, T. Methfessel, J. Mueller, M. Lang, M. Huth,M. Jourdan, and H.-J. Elmers, (2014), arXiv:1410.5245 [cond-mat.str-el]

[16]. M. Sing, U. Schwingenschlögl, R. Claessen, M. Dressel, and C. S. Jacobsen, Phys. Rev. B **67**, 125402 (2003).

[17]. J.J. Yeh and I. Lindau, At.Data Nucl.Data Tables, **32**, 1(1985).

[18]. A. Sekiyama, T. Susaki, A. Fujimori, T. Sasaki, N. Toyota, T. Kondo, G. Saito, M. Tsunekawa, T. Iwasaki, T. Muro, T. Matsushita, S. Suga, H. Ishii, T. Miyahara, Phys. Rev. B **56**, 9082 (1997).

[19]. R. Liu, H. Ding, J. C. Campuzano, H. H. Wang, J. M. Williams, K. D. Carlson, Phys. Rev. B **51**, 13000 (1995).

[20]. J. E. Downes, K.E. Smith, A. Y. Matsuura, I. Lindau, J. A. Schlueter, Surf. Science, **551**, 219 (2004).

[21]. T. Kiss, A. Chainani, H.M. Yamamoto, T. Miyazaki, T. Akimoto, T. Shimojima, K. Ishizaka, S. Watanabe, C.-T. Chen, A. Fukaya, R. Kato, S. Shin, Nature Communications **3**, 1089 (2012).

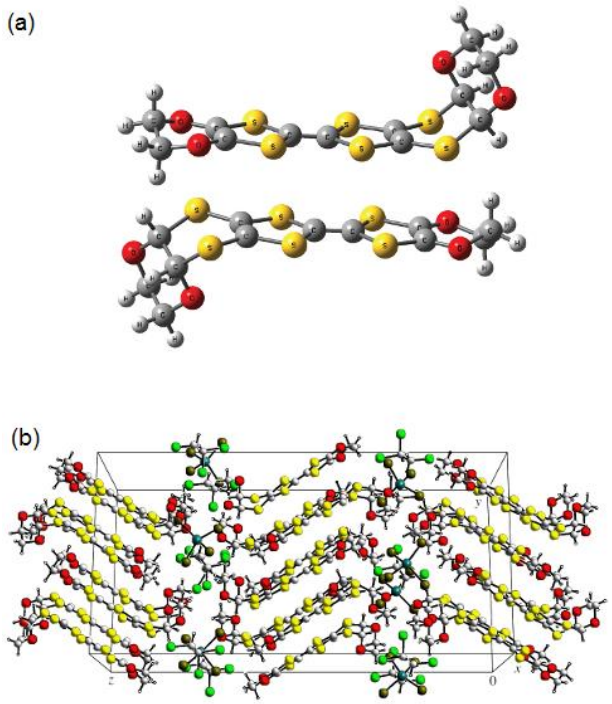

FIG. 1.Molecular dimer DOEO (a) and $(DOEO)_4[HgBr_4]\cdot TCE$ crystal (b) structures revealed in Refs [6-9].

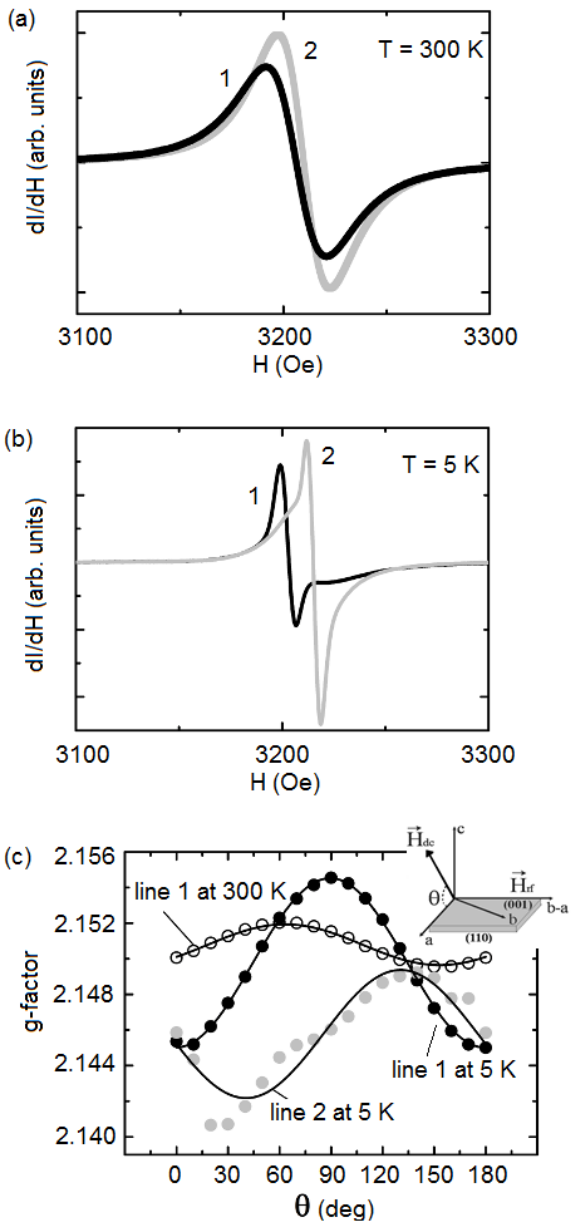

FIG.2. (a, b) ESR spectra of a $(DOEO)_4[HgBr_4]\cdot TCE$ crystal at T = 300 K (a) and 5 K (b). In both panels the angle between the magnetic field and the *ab* crystal plane is θ = 70°(grey lines) and θ = 150° (black lines). (c) The "out-of-plane" angular dependence of *g*-factors of a $(DOEO)_4[HgBr_4]\cdot TCE$ crystal obtained from the ESR spectra at T = 5 K for line *1* (black symbols) and line *2* (grey symbols). Open symbols give the angular dependence of line *1* at T = 300 K. The inset shows the orientation of the microwave and static magnetic field of the spectrometer with respect to the crystal, as well as the direction of sample rotation. The solid lines are approximations of the angular dependences by the spin Hamiltonian corresponding to axial symmetry. [10]

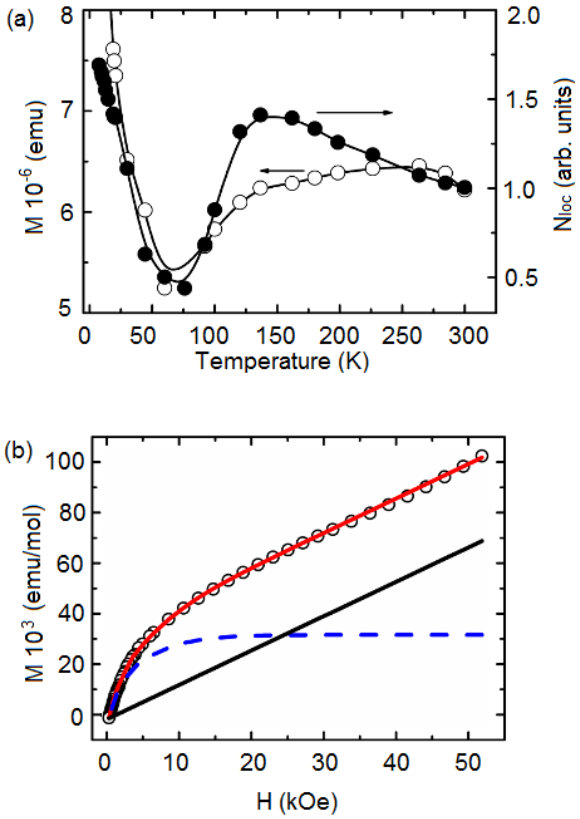

FIG.3. (a) Temperature dependencies of the magnetic moment of the sample *M* in constant magnetic field 1 kOe and number of localized charge carriers N_{loc} recalculated from resistivity, (b) Field dependence of magnetic moment of $(DOEO)_4[HgBr_4]\cdot TCE$ crystal at 2 K. The solid line shows the approximation of the magnetic moment with sum of the Brillouin function (dashed line) and linear dependence.

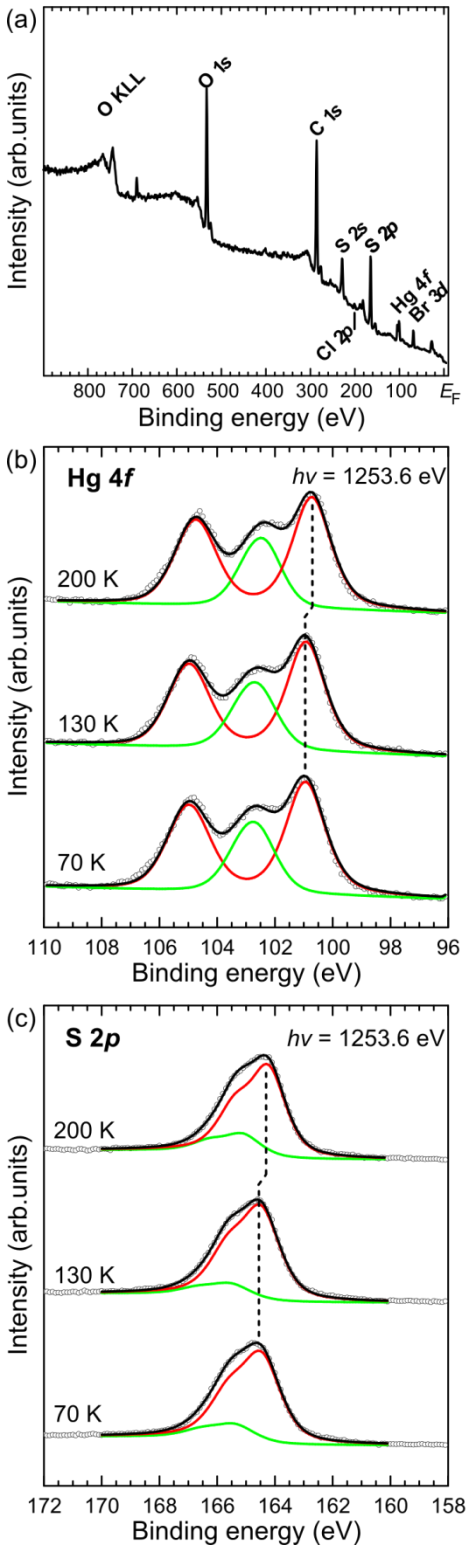

FIG. 4. (a) Survey XPS spectrum of the surface of the $(DOEO)_4[HgBr_4]\cdot TCE$ crystal taken at room temperature, (b) an example of the temperature behavior of Hg 4f core-level XPS spectra at T = 200 (top), 130 (center) and 70 K (bottom), (c) example of the S2p core level spectrum decomposition at T = 200 (top), 130 (center) and 70 K (bottom).

Circles show the experimental results, solid lines represent the deconvolution of the spectra by a least squares fit. In both cases the sum spectrum of the deconvoluted peaks agrees perfectly with experiment.

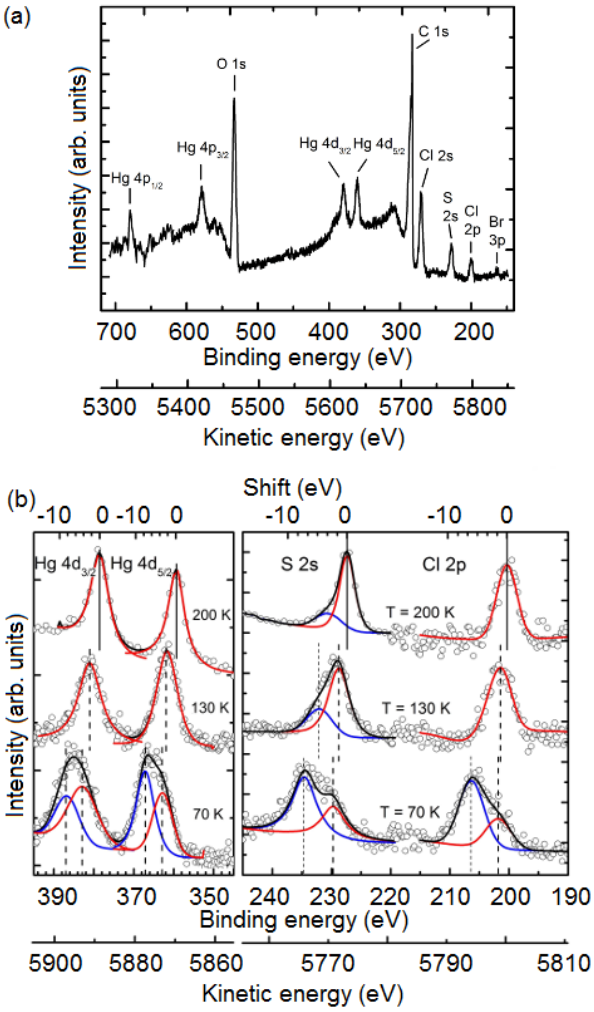

FIG. 5. (a) Survey HAXPES core level spectrum of $(DOEO)_4[HgBr_4]\cdot TCE$ taken at room temperature; (b) Mercury 4d (left panel), sulfur 2s and chlorine 2p (right panel) HAXPES core-level spectra for three temperatures of $(DOEO)_4[HgBr_4]\cdot TCE$: T = 200 (top), 130 (center) and 70 K (bottom). Circles show the experimental results, solid lines represent the deconvolution of the spectra by a least squares fit. Vertical lines show the center positions of the deconvoluted peaks.

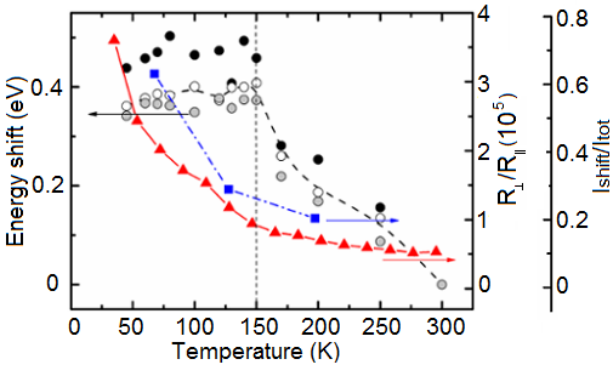

FIG. 6. The temperature dependencies of the shift of core levels of Hg (black circles), S (gray circles) and Br (white circles) in $(DOEO)_4[HgBr_4]TCE$ crystal, relative peak intensity of S 2s (blue squares, see Fig. 5b) and electrical anisotropy parameter (see text) $R_\perp/R_\parallel$ (red triangles). Full, dashed and dash-dot lines are to guide the eye, denoting the anisotropy parameter, the Hg and S core level positions, and the intensity ratio of the shifted S 2s HAXPES signal, respectively.

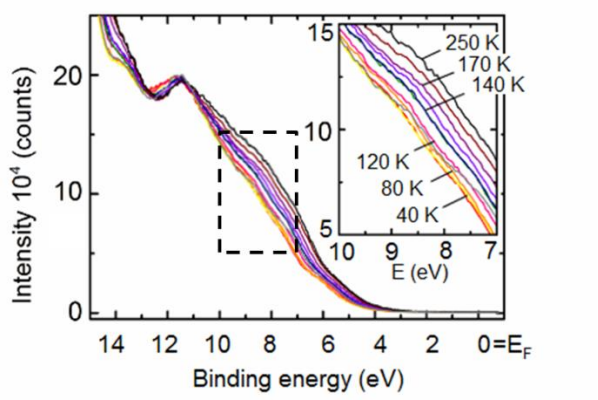

FIG. 7.UPS spectra of$(DOEO)_4[HgBr_4]TCE$ crystal recorded at different temperatures with a He I source ($h\upsilon$ = 21.2 eV). The area marked by the dashed rectangle is enlarged in the inset.

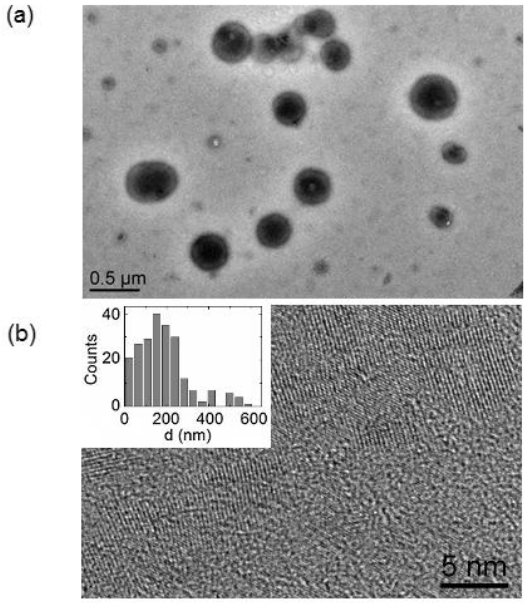

FIG. 8. TEM images of the large (a) and small (b) clusters in the crystals. The inset shows the size distribution of clusters.